Final results of an experimental study of a large area planar drift chamber filled with a He–based mixture

M. Agnello[a,b], P. A. Amaudruz[c], *E. Botta[b], T. Bressani[b,d], L. Busso[b,e], D. Calvo[b], P. Cerello[b], C. Fanara[a], A. Feliciello[b], A. Filippi[b], F. Iazzi[a,b], S. Marcello[b], B. Minetti[a,b], N. Mirfakhrai[f] O. Morra[b,g], A. Raimondo[b,d], E. Rossetto[b], A. Sharma[b], A. Zenoni[h,i]

[a] *Dipartimento di Fisica del Politecnico di Torino and INFN, Sezione di Torino, C.so Duca degli Abruzzi 24, I–10124 Torino, Italy*
[b] *INFN, Sez. di Torino, Via Giuria 1, I–10125 Torino, Italy.*
[c] *TRIUMF, 4004 Wesbrook Mall, Vancouver, BC, V6T 2A3, Canada*
[d] *Dipartimento di Fisica Sperimentale, Università di Torino, and INFN, Sezione di Torino, Via P. Giuria 1, I–10125 Torino, Italy.*
[e] *Dipartimento di Fisica Generale, Università di Torino, and INFN, Sezione di Torino, Via P. Giuria 1, I–10125 Torino, Italy.*
[f] *Department of Physics, Shahid Beheshty University, 19834 Teheran, Iran*
[g] *CNR, Istituto di Cosmogeofisica, C.so Fiume 4, I–10131 Torino, Italy*
[h] *Dipartimento di Chimica e Fisica per i Materiali, Universita' di Brescia, Via Valotti 9, I–25133 Brescia, Italy*
[i] *INFN, Sezione di Pavia, Via Bassi 6, I–27120 Pavia, Italy*

Abstract

This paper reports the final results of an accurate and complete experimental study of the performance of a large area ($1150 \times 566\, mm^2$) planar drift chamber filled with a $He - iC_4H_{10}\,(70\% - 30\%)$ mixture. Sixteen chambers of this type will constitute the elements of the central part of the tracking device of FINUDA, one of the two spectrometers approved for running at DAΦNE. The measured spatial resolution across the full drift cell ranges from 80 to $120\,\mu$m for particles at normal incidence angle, and the measured spatial resolution along the sense wire, as measured by the charge division method, was better than 1% of the wire length. Efficiency, space-time relationship, long term stability and Lorentz angle

*Corresponding author. Fax: +39 11 6707324, e–mail: botta@to.infn.it.

were measured as well. Particular care was devoted to the study of the spatial resolution as a function of the incidence angle. The conclusion of this study is that the chamber performances are the same or better than those obtained with Ar–based mixtures.

PACS 29.40.G, Keywords: tracking, drift, Helium, low–mass, resolution.

1 Introduction

This paper reports the final results of an accurate and complete experimental study of the performance of a large area $(1150 \times 566)\ mm^2$ planar drift chamber operating with a $He - iC_4H_{10}\,(70\% - 30\%)$ mixture. The measurements were performed during two periods of run at a test beam at the CERN PS. First results from the data collected during the first period were already published [1].

The study was motivated by the fact that chambers of this kind will constitute the central element of the tracking device of the FINUDA spectrometer. FINUDA (acronym for FIsica NUcleare a DAΦNE) is one of two magnetic spectrometers approved for running at DAΦNE, the high luminosity ($\mathcal{L} = 5 \times 10^{32}\, cm^{-2}\, s^{-1}$) ϕ-factory; the construction was approved in 1990 by INFN, Italy, at the Laboratori Nazionali di Frascati (LNF) and the commissioning stage will start at the beginning of 1997.

The physics goal of FINUDA is the study of the production of Λ-hypernuclei from the (K^-_{stop}, π^-) reaction on nuclear targets and of their subsequent decay [2]. The experiment exploits the fact that the very low energy ($\sim 16\, MeV$) K^- from the Φ-decay may be stopped in very thin targets [2], allowing unprecedented production rate and energy resolution on the final hypernuclear levels if a large acceptance ($\geq 2\,\pi\, sr$) and good momentum resolution ($\Delta p/p\ \leq 0.3\,\% FWHM$) magnetic spectrometer is built around the interaction region.

Following a long period of studies and simulations the final design of the FINUDA spectrometer was discussed and approved [3]. Fig. 1a) shows a pictorial view of the spectrometer. It consists of a superconducting solenoid, of $1385\, mm$ radius and $2770\, mm$ length, providing a field of induction $B = 1.1\, T$, constant within 1% over the tracking volume, which has a clepsydra shape. The tracking of the particles emitted from the nuclear targets (π^- of $\sim 250 - 270\, MeV/c$) is performed by three different kinds of sub-detectors: a layer of Si μ-strip detectors, two layers of low mass drift chambers ($LMDCs$) and six layers of straw-tubes (ST) in a stereo assembly. The choice of this combination of different sub-detectors was found better than that of a unique, homogeneous detector (a Time Projection Chamber [3, 4] or a multi-cell Drift Chamber, like that used for KLOE [5], the other DAΦNE experiment) with respect to the intrinsic spatial resolution and then on the final momentum resolution.

The full tracking device is immersed into a Helium atmosphere for minimizing multiple Coulomb scattering. For that purpose, the mylar windows of the drift chambers must be very thin ($36\,\mu m$ in total for each chamber) and the gas mixture must be of low–mass with Helium as main component. Furthermore, the thickness of the chamber had to be reduced at minimum, and we decided to solve the left/right ambiguity by the method of the doublet of sense wires [6]. Finally, since maximum spatial resolution was required only in the (R-ϕ) plane, we decided to measure the orthogonal coordinate (along the wire) by the charge division method. From the Monte Carlo simulation of the complete apparatus it is seen that the particles (π^-s) emitted from nuclear targets surrounding the interaction region (we remind that FINUDA is the first, unique example of a nuclear physics experiment carried out at a collider), cross the two layers of $LMDCs$, arranged into two octagonal arrays rotated by a suitable angle ($11°$, see Fig. 1 b) for maximizing the acceptance for π^-, with quite large angles. The $LMDCs$ are held into position by a stiff and precisely machined casted Aluminum structure, called clepsydra in Fig. 1a). Fig. 2 shows the distributions of the angles that the π^-s form with the isochronous lines of the two layers of $LMDCs$, of dimensions $(1230 \times 396)\,mm^2$ and $(1870 \times 686)\,mm^2$ respectively.

It is known [7] that the spatial resolution of the $LMDCs$ drastically worsens as a function of this angle but no measurements were performed so far with He–based mixtures. Therefore a particular care was devoted to the detailed study of this effect.

Summarizing, a careful study of the performance of large area planar drift chambers operated with He-based mixture was mandatory before the starting-up of the spectrometer construction, since the spatial resolution, expected to be around $100\,\mu m$ [2], was a non-negotiable requirement.

2 Chamber structure and drift cell layout

The operation of a drift chamber, aiming to reach the best localization accuracy, largely depends on the precise knowledge of the space-time relationship, which in turn depends on the gas mixture employed and the electric field in the chamber. The use of Helium as main component in mixtures for drift chambers has received an increasing attention in the last few years [8, 9, 10, 11, 12, 13, 14, 15, 16] for several reasons that will be summarized at the end of this section. Drift velocities in He-based mixtures were found generally non-saturated even up to electric fields of almost $2\,kV/cm$. To compensate for this effect the electric field in the sensitive region must be as uniform as possible.

Fig. 3 shows an exploded view of the mechanical layout of the chamber called PLMDC (Prototype Low Mass Drift Chamber) in the following. It consists of five fiber glass frames supporting mylar windows, cathode and anode wires, and two external aluminum frames necessary to reinforce the structure and to give the exact position for the anode and cathode frames with locating pegs. The frames are sandwiched and strongly clamped with screws in order to obtain a rigid structure and squash the sealant O-rings. The frames are symmetrically sandwiched with respect to the anode frame.

Fig. 4 shows in detail the disposition of wires and mylar sheets constituting the cell. The drift cell design resembles the one originally proposed in [7]: the cell is built up of two parallel layers of cathode wires at a relative distance of $6\,mm$ with a doublet of anode wires placed in the center. The cathode wires spacing has been opted to be $1\,mm$, so that the electric field was not too modulated close to the cathode plane, while keeping ease of machining, fabrication of the printed circuit board and soldering. The cathode wires, made of Cu-Be, have a diameter of $50\,\mu m$ and are soldered with a tension of $1.1\,N$, a factor nine less than the limit for electrostatic stability. The calculated gravitational sagitta was $24\,\mu m$. Wires of the same type were used as field wires in the anode plane, spaced by $50\,mm$. The anodes were made by a doublet of adjacent stainless steel wires, with a diameter of $25\,\mu m$ and spaced by $200\,\mu m$. They were soldered on the printed board with a tension of $0.55\,N$, a factor four less than the limit for electrostatic stability. The calculated gravitational sagitta was $10\,\mu m$. Small araldite glue droplets were put at regular intervals of $11.5\,cm$, to maintain the sagitta due to electrostatic repulsion force within $40\,\mu m$: without droplets the sagitta would reach the unacceptable value of $3\,mm$. The anode doublets were spaced by $50\,mm$. The specific resistivity of anode wires was $1770\,\Omega\,m^{-1}$, high enough to use the charge-division method with a good precision.

The two cover frames are designed to close the drift region in order to permit the gas to flow inside the chamber and to get a better uniformity of the electric field. For this purpose on the cover frame an aluminized mylar foil, $12\,\mu m$ thick, was glued with a linear tension of about 588 N/m with the aluminum layer ($\sim$ 300 Å) facing inwards the drift cell. A $6\,\mu m$ thick aluminized mylar sheet was glued on the other side, with the Al coating facing outward the chamber. In this way we obtained a good electric contact with the ground. On the other cover frame this sheet was replaced by a $50\,\mu m$, not aluminized, mylar sheet, allowing the measurement by optical methods of the displacement of the internal mylar sheet due to a small differential pressure experienced by the gas flow.

A series of grooves, designed to optimize the gas flow inside the chamber, are placed on both ends of the anode plane, as shown in Fig. 3. The gas directly enters the drift volume, defined by the ground aluminized mylar planes (see Fig. 4), on one end, and goes out at the other end through the grooves; then it enters the two external volumes between each ground plane and the corresponding external mylar plane, flowing in the opposite direction. This flow guarantees that the internal pressure is kept higher with respect to that of the external volumes, and the internal mylar sheet cannot be displaced towards the cathode wires, thus avoiding the possibility of electric discharges.

A careful study of how possible displacements of the different elements from the correct position could affect the final performance on the spatial resolution of the chamber was performed [17] by means of the GARFIELD code [18]. The displacements can be due to mechanical positioning precision of the wires or can be a consequence of the electrostatic forces between the anode pair, anode and cathode and ground planes. In particular, situations with different values of displacements of, respectively, one anode wire, all the wires of a cathode plane, the field wire, a ground plane or combinations of these have been considered for some typical track incidence angles. Full results are given in [17]. Fig. 5 and Fig. 6 show the difference of the arrival times of the electrons for anode and cathode displacements, while Fig. 7 reports the deviation in the reconstructed position determined by a movement of a ground plane. The conclusion of this study was that the mechanical tolerances requested on the chambers ensured to maintain the spatial resolution within the requirements of the experiment.

As mentioned in the introduction, the gas mixture must have the following characteristics in order to fulfill the requirements:

- low mass and density
- large radiation length
- small coefficient of longitudinal diffusion
- large number of primary and total ion-electron pairs
- low drift velocities
- small Lorentz angle
- immunity from internal contamination (essentially He of the He bag)
- to be non corrosive

Following the results [14] of a calculation of the features of He–based mixtures, we evaluated that the $He-iC_4H_{10}(70\%-30\%)$ mixture was the best candidate. Tables 1 and 2 summarize the calculated parameters for some He–based mixtures [14]. A preliminary study carried out with radioactive sources [3] ensured us that the $He-iC_4H_{10}\,(70\%-30\%)$ choice was good in terms of operation stability and reliability and the major part of the accurate study with beam was performed with this mixture.

The GARFIELD code has also been utilized to evaluate the influence on the chamber behaviour of the variation of the gas mixture composition and of the variation of temperature and pressure. In correspondence to variations of, separately, 1% in the mixture percentages, $1\,K$ in temperature and $\sim$ 40 Torr in pressure, that are typical values that can be found in operating conditions, the drift velocity and Lorentz angle show variations well within the limits of our requested precisions [17].

3 Experimental apparatus

Fig. 8 shows the experimental layout, installed at the T10 beam test area at the CERN PS: it is the set-up for the second period of run, slightly different from that for the first period, already described in [1]. In addition to the distances between the detectors and the dimensions of the trigger scintillators, the main difference was that the chamber could be rotated along an axis parallel to the anode wires. Then the spatial resolution for a particle crossing the chamber with an angle respect to the isochronous lines could be carefully studied. The PLMDC was mounted on a mechanical support allowing a displacement both in the x (along the drift cell length) and z (along the wire) directions over the full chamber dimensions, with a precision of $\pm 100\,\mu m$. The precision on the rotation angle was $\pm\, 0.5°$. The tracking of the particles crossing the PLMDC was performed by means of two drift chambers of smaller dimension (DR_1 and DR_2) with bi-dimensional read-out, placed upstream and downstream the PLMDC, flushed by the same mixture, with the same drift geometry and equipped with the same electronics.

The trigger logic is shown in Fig. 9. The trigger signal is given by the coincidence of S_1, S_2 and S_3 scintillators. The signal from S_4 could be inserted in the coincidence to select via hardware a beam collimated in the z direction.

The selected beam momentum was $5\,GeV/c$, to avoid corrections due to the multiple Coulomb scattering, and the trigger rate was selected through the beam-collimator to be ~ 170 particles (mostly π^-)/burst. These conditions ensured a quite low double hit probability ($< 10\%$) due to the time structure of the beam (burst duration $= 300\,ms$).

Each end of each sense wire of the PLMDC was connected to an ADC LeCroy 2249W and TDC LeCroy 2228A by an electronic chain consisting of a low noise home made amplifier directly coupled to the wire and a discriminator $\sim 50\,m$ far in the counting hut. It is well known that the performance of a drift chamber, and in particular the z-determination by the charge division method, is related, among other parameters, to the amplifier signal/noise ratio. To this purpose we used in our tests two arrangements. The first was the conventional one of coupling each end of each anode to an amplifier, and with this arrangement we obtained most of the results reported in [1]. The second was that of coupling together the information from the inputs of each element of the anode doublet by means of a twin amplifier. A true negative pulse on a wire of the doublet produces an induced positive pulse with an amplitude ~ 0.8 times the amplitude of the true signal on the other wire. The twin amplifier, working on both signals of the anode doublet, adds to the signal from one wire that from the adjacent one, inverted. Then, the twin amplifier gives for a true signal a value that is 1.8 times that with the normal coupling. The coupling among the inputs also produces an increase of the uncorrelated noise, which is $\sqrt{2}$ of the noise of a single wire. Thus a net increase of a factor $1.8/\sqrt{2} \sim 1.3$ on the signal/noise ratio is obtained by this method. A further, important advantage of the technique is that common noise on both wires of the doublet (like environmental e.m. noise) is automatically canceled at the input stage. A detailed account of this method is given in [19].

The data acquisition (DAQ) system has been designed to optimize the event acquisition rate according to the beam time structure. The data taking was based on a VME Tecnint 3032 cpu connected to a CAMAC crate via a CBD 8210 Camac Branch Driver. The run-control program was running on a 3100/76 VaxStation connected via Ethernet to the DAQ cpu. To minimize the DAQ dead time the data were stored in the internal memory of the cpu during the burst. The inter-burst time (15 sec) was utilized to transfer via Ethernet the data to a VaxStation memory buffer shared between the monitoring and the mass storage writing processes. The acquisition rate obtained was $\sim$ 150 events/burst. Monitoring programs performed a preliminary analysis, creating suitable n–tuples. The most significative quantities were continuously displayed utilizing PAW [20] as a presenter.

4 Experimental results

We do not report here for brevity straightforward measurements concerning H.V. plateaux and so on; they can be found in [21]. Typical working condition for the measurements that will be reported in the following are $-3750\,V$ for the drift potential, corresponding to a drift field of $1440\,V/cm$ and $+1850\,V$ for the anode pair voltage, about $150\,V$ beyond the plateau knee.

The fine scanning of the drift cell was performed by using the time information from DR1 and DR2 as a collimator selecting on PLMDC a beam of dimensions that could be varied as required in the off-line analysis, following the technique described in detail in [7, 22].

4.1 Efficiency

A careful mapping of the detection efficiency ϵ over the full cell volume and as a function of the angles of rotation around the x axis direction (θ) and z axis direction (β) was performed. In chambers using the doublet of sense wires at high positive voltage, the decoupling capacitor produces an overshoot of polarity opposite to that of the (direct or induced) signal. Then, sometimes the doublet of sense wires gives a pair of signals, one corresponding to the true one, the other to the overshoot of the induced signal on the adjacent wire. In our conditions, about 3.5% of the events showed this structure. However this value could be lowered to less than 1% by analysing the ADC and TDC responses of the doublet of wires: the true signal was defined as the one giving the larger ADC and shorter TDC information.

Due to the beam time structure, 5% to 10% of triggers were due to pile-up events: they were eliminated by a careful analysis of the topology of events recorded by the adjacent cells. Full details of this procedure may be found in [21].

The measured efficiency ϵ across the drift cell was $(99.3 \pm 0.2)\%$, except in the proximity of the glue droplets along the doublet of sense wires, where it falls to $(\sim 86.1 \pm 0.2)\%$. This local inefficiency was limited to a spatial region lower than 1 cm for each droplet along the wire. The integrated efficiency over the full drift cell is then $(98.1 \pm 0.2)\%$. These results are fully consistent with those measured with Ar-based mixtures [7]. No variation was observed as a function of the θ angle (up to 40°). The corresponding histograms were already reported in [1]. In the second run we measured also ϵ as a function of the β angle. Fig. 10 reports the results. As expected from the fact that particles crossing the chamber along inclined lines deposit a large amount of energy, ϵ always reaches values exceeding 99%, except in the proximity of the field wire (≤ 2 mm) for $\beta = 40°$. This is due to the fact that the particle crosses only a reduced part of the cell, and therefore the signal lies below the discriminator threshold.

4.2 Spatial resolution

The spatial resolution was measured by the usual method of the residuals, under the assumption that the contributions of the three chambers, flushed by the same gas, equipped with the same electronics and with similar cell structure were equal. Fig. 11 shows a typical example of a distribution of residuals, well fitted to a gaussian. The measured σ_{res} at each position, divided by $\sqrt{(2/3)}$, provided the local spatial resolution σ_{loc}, reported in the following. We studied the spatial resolution variation as measured by each one of the two TDCs connected to each of the sense wire ends, and also using the average time from the wire (AT) obtained via software by $(TDC1 + TDC2)/2$. No significant variations among the different measurements were observed, and therefore we report for simplicity only σ_{loc} as measured by AT of each wire.

Fig. 12 shows the variation of σ_{loc} as a function of the distance from the anode wire: measurements performed in both 1994 and 1995 runs are shown. We expect that the behaviour of σ_{loc} is well reproduced by quadratically adding three contributions:

1. $\sigma_{el} \sim a$, representing the contribution from the electronic chain (preamplifier, discriminator, TDC, ...)

2. $\sigma_{diff} \sim 0.91\sigma_L \frac{\sqrt{x}}{\sqrt{\log(n)}}$ [23] in which σ_L represents the single electron longitudinal space diffusion corresponding to a 1 cm drift length, x is the distance (in cm) from the wire and n the total number of ionization electrons.

3. $\sigma_{pairs} = ce^{-cx}$, representing the statistics of the electrons from the primary ionization, c being the number of primary electrons;

A fit of the experimental distribution to the function:

$$\sigma_{loc}(x) = [a^2 + (b\sqrt{x})^2 + (ce^{-cx})^2]^{1/2} \tag{1}$$

is represented in Fig. 12 a), together with the behaviour of the different contributions. For this first fit we used $c = 10.8$ (as deduced from [24], table 1, over a distance of $6\,mm$). We deduced then $\sigma_{el} = (71.1 \pm 1.2)\,\mu m$ and for σ_L a value of $(125.2 \pm 2.7)\,\mu m$, with a χ^2/ν of 4.25. This fit does not reproduce very well the behaviour of σ_{loc} for small distances. A better fit is obtained by using as fitting function:

$$\sigma_{loc}(x) = [a^2 + (b\sqrt{x})^2 + (de^{-cx})^2]^{1/2} \tag{2}$$

in which also the parameter d was allowed to vary (Fig. 12 b). This circumstance is not surprising if we consider that the inadequacy of the first fit was clearly evident near the anode wire, in a region critical both for the electric field distribution and for the variation of the drift velocity. We deduced from this fit $\sigma_{el} = (66.5 \pm 1.3)\,\mu$m and for σ_L a value of $(133.2 \pm 2.7)\,\mu$m with a χ^2/ν of 2.57. We notice however that the value of σ_L inferred from the second fit is in worse agreement with the calculated one (117.6 μm, see table 1).

We also measured the above distribution of $\sigma_{loc}(x)$ at different positions along the anode wire (z-axis) and for each position, at different values of the angle θ (up to $40°$ in step of $10°$). As expected, we found no variations within the experimental errors.

An extensive study of the variation of σ_{loc} as a function of the angle β, expected to be more critical, was furthermore performed: Fig. 13 summarizes the results of such a study. Here the experimental data are presented as the ratio of the measured $\sigma_{loc}(x, \beta)$ to the measured $\sigma_{loc}(x, 0)$. Notice that, by increasing the rotation angle we could not reach the largest values of x (near the anode wire) due to the fact that mechanical axis of rotation of the chambers did not coincide with the axis of rotation along the drift cell.

As reported in previous studies on chambers working with Ar-based mixtures [7], we observe a degradation of the relative resolution increasing β, reaching a maximum around the middle of the cell ($x = 10 \div 15\,mm$). From all the results of σ_{loc} so far reported we derived the following parametrization for $\sigma_{loc}(x, y, \beta, \theta)$:

$$\sigma_{loc}(x, y, \beta, \theta) = \sigma_{loc}(x) R(\beta) \tag{3}$$

in which $\sigma_{loc}(x)$ was given by (2) and $R(\beta)$ was fitted to a parabolic function:

$$R(\beta) = \frac{\sigma(\beta)}{\sigma(0°)} = e + f\beta + g\beta^2 \tag{4}$$

The fit to (4) from the experimental data (Fig. 13) was performed using the averaged values of $\frac{\sigma(\beta)}{\sigma(0°)}$ in the interval $5 \leq x \leq 15\,mm$ and the result is shown in Fig. 14, reporting also the best fit values for e, f, g.

4.3 Resolution along the wire

The improvement obtained in using a twin amplifier instead of a single one is clearly visible in Fig. 15. It shows the precision on the z-measurement with the use of a single amplifier coupled to each wire compared to that obtained with the twin amplifier. The measurements were performed with the beam at the center of the cell ($x = 12\,mm$) at $\theta, \beta = 0°$. The improvement is 30% at the center of the wire ($z = 0$) and 50% (at $z = 50\,cm$). This observation led us to choose the twin amplifier option for all the further measurements and for the general use in the FINUDA spectrometer.

Another source of error in the determination of the z coordinate is associated to the arrangement of having the sense wires at a positive H.V., with the consequent need of decoupling capacitors for the read-out. Whereas no influence is expected on the TDC signal (and then on the x-coordinate measurement), the situation is quite different for the ADC signal. In this case, in fact, the integration gate for the ADC has to be opened for a time corresponding to the maximum drift time along the cell ($\sim$ 800 ns in our case), and the charge collected by the ADC is quite a complicated function, apart from the electric characteristics, of the arrival time of the electronic avalanche and of the gate duration. Very schematically, the z-coordinate would be given, at a first approximation (without considering the effect of the decoupling capacitors) by:

$$z = \frac{q_R - q_L}{q_R + q_L} k \tag{5}$$

where q_R and q_L are the integrated charges collected on the two sides of the wire (L for Left, R for Right) and k a constant defined by:

$$k = \frac{L}{2} + \frac{Z_i}{\rho} \tag{6}$$

in which L is the total length of the wire, Z_i is the amplifier input impedance and ρ the specific resistance of the wire.

The fact that (5) and (6) are clearly unadequate to accurately describe the behaviour of our system can be clearly seen from Fig. 16. The measurements were done with the beam at $x = 12\,mm$ and at the values of z shown by the figure. The relationship between measured and calculated points is linear, but k is 1.256 ± 0.050 times the value given by (6).

The compression factor on the value of the z-coordinate is a function of the arrival time of the electronic avalanche and of the gate duration. A quite realistic model was developed, and will be soon published. Here we only remind the general features and conclusions. A first remark is that a better determination could be obtained by looking for a parametrization of k as a function of z, but always integrated over the full gate duration ($1.5\,\mu sec$). The first parametrization we found was:

$$k_{mean}(z) = h + lz + mz^2 \tag{7}$$

with

$$
\begin{aligned}
h &= (0.123 \pm 0.016) \times 10^{1} \\
l &= (-0.9 \pm 1.1) \times 10^{-2} \\
m &= (0.24 \pm 0.18) \times 10^{-3}
\end{aligned}
\tag{8}
$$

and we obtained a slight improvement in the resolution on the z-coordinate.

A very substantial improvement was obtained by using a gate duration of $200\,ns$, and selecting only the relevant part of the ADC spectrum. We obtained a very impressive result, as shown in Fig. 17. A software correction, corresponding in principle to the above hardware operation was found not so useful. Table 3 summarizes the results on the z-coordinate determination as obtained with the different approaches. The fits to the z experimental distributions were obtained by using a Lorentzian function instead of a Gaussian one, as expected by the formula giving z as a function of two functions exhibiting a Poisson distribution. In the table the quoted errors are obtained as the width of the Lorentzian fit divided by 2.36.

The precision on the z-measurement by the charge division method is expected to improve as a function of both the angles θ and ϕ, due the larger deposit of energy in the cell, and we checked this effect at some points and for different β, θ angles.

4.4 Determination of the Space–Time relationship

The main characteristics of the $He - iC_4H_{10}$ gas mixture were all calculated in advance, but we checked them with dedicated measurement. The most important one is the determination of the drift velocity $v(t)$, and consequently of the Space-Time relationship. A first determination, performed with cosmic rays and sources irradiating uniformously a drift cell ensured us that the calculated average velocity agreed within 5% with the measured value. However, we performed a dedicated measurement with the set-up of Fig. 8, by applying the so-called displacement method [25]. The results are shown by Fig. 18. We may observe that the calculated values agree with the measured ones within some %. A fit of the differential drift velocity $v(t)$ to a polynomial function showed that a linear expression like:

$$v(t) = n + pt \tag{9}$$

with coefficients

$$
\begin{aligned}
n &= (35.4 \pm 1.0)\ \mu m/ns \\
p &= (-5.1 \pm 1.3) \times 10^{-3}\ \mu m/ns^2
\end{aligned}
$$

was good enough to reproduce the data within the given errors.

4.5 Determination of the Lorentz angle

Given the dimension of the chamber, we could not perform a direct measurement of the Lorentz angle (ψ) with beam. However, by using the apparatus originally described in [26] we verified, with measurements in some selected conditions, the reliability of the calculation for the $He - iC_4H_{10}$ ($70 - 30\%$) mixture. 5.9 KeV photons from a ^{55}Fe source were utilized. Knowing the dependance of ψ on the applied electric and magnetic fields, we measured, at fixed ψ, the values of $\vec{B}$ corresponding to different $\vec{E}$ and we found that measured and calculated values of $\vec{B}$ agreed within 2%.

4.6 Long Duration Test

After completion of the tests with the beam, we checked the long term stability of PLMDC in order to ascertain possible effects of ageing. To this purpose we installed PLMDC at a test station located at Laboratorio Tecnologico, INFN, Sezione di Torino. The chamber was irradiated continuously with a ^{106}Ru source (activity = 10^4 Bq). A selected small volume in the drift cell was defined by the coincidence of two thin scintillators placed upstream and downstream of the chamber. The amplification of the chamber and the average drift velocity, that are the most important parameters, were continuously monitored by means of the integral ADC and TDC spectra. The measurement lasted for more than 4000 hours.

PLMDC worked without interruptions for all the above period showing no major drawbacks like sparkings or variations of the average drift velocity. The only effect we observed was a variation of the amplification gain as a function of the atmospheric pressure, as expected.

5 Conclusions

We have performed a quite complete study with beam and in laboratory of the performance of a large area planar drift chamber operating with a $He - iC_4H_{10}$ ($70 - 30\%$) mixture. The following features were observed:

1. the integrated efficiency of the chamber is $(98.1 \pm 0.2)\%$. Local inefficiencies of 14% are observed only in the vicinity of the glue droplets holding together the doublet of sense wires;

2. the spatial resolution across the full drift cell ranges from 80 to 120 μm for particles at normal incidence angles, increasing to 300 μm for incidence angles of $55°$;

3. the determination of the z–coordinate along the wire is of the order of 1% of the wire length . It can be pushed to $\sim$ 0.3% using dedicated hardware

corrections;

4. the measured parameters (drift velocity, space–time relationship, Lorentz angle) agree within $2-3\%$ with the calculated ones;

5. no ageing effect were observed over a period of 4000 hours.

The final conclusion is then that He–based mixtures, in particular the $He-$ $-iC_4H_{10}$ $(70-30\%)$ one allow to reach the same performances of drift chambers than Ar–based mixtures, and that they are obvious candidate in experiments affected by a strong e.m. background, like at (e^+ e^-) colliders. As a matter of fact, following the results so far described, we constructed all the 20 chambers for the FINUDA apparatus.

6 Acknowledgements

We are warmly indebted to Prof. F. Sauli for his precious help and advice. Mr. R. Bouclier and Mr. G. Million are gratefully acknowledged for their support during the beam tests. We express our gratitude to Mr. B. Casavecchia, Mr. L. Simonetti and Mr. A. Piantoni for the skillful assistance in the construction and operation of the chamber.

References

[1] M. Agnello *et al.*, *Nucl. Instr. Meth.* **367** (1995), 100–103.

[2] The FINUDA Collaboration, FINUDA, a Detector for Nuclear Physics at DAΦNE, Report LNF 93/021 (1993).

[3] The FINUDA Collaboration, FINUDA Technical Report, Frascati Internal Report LNF 95/024 (IR), May 18 1995.

[4] E. Rossetto and A. Sharma in *Proceedings* of the 8^{th} Winter School on Hadronic Physics, T. Bressani, M. Gibilisco, G. Preparata Eds., World Scientific, Singapore, 1993, p. 439.

[5] The KLOE Collaboration,"The Kloe Central Drift Chamber", LNF–94/028(IR).

[6] G. Charpak and F. Sauli, *Nucl. Instr. Meth.* **107** (1973), 371.

[7] A. Breskin *et al.*, *Nucl. Instr. Meth.* **119** (1974), 9–28.

[8] W. Zimmermann *et al.*, *Nucl. Instr. Meth.* **A 243** (1986),86.

[9] F. Grancagnolo, *Nucl. Instr. Meth.* **A 277** (1989), 110.

[10] V. Cindro *et al.*, *Nucl. Instr. Meth.* **A 309** (1991), 411.

[11] S. M. Playfer *et al.*, *Nucl. Instr. Meth.* **A 315** (1992), 494–501.

[12] P. R. Burchat *et al.*, *Nucl. Instr. Meth.* **A 316** (1992), 217.

[13] S. Uno *et al.*, *Nucl. Instr. Meth.* **A 330** (1993), 55.

[14] A. Sharma and F. Sauli, *Nucl. Instr. Meth.* **A 350** (1994), 470–477.

[15] P. Bernardini, *Nucl. Instr. Meth.* **A 355** (1995), 428.

[16] K. K. Gan *et al.*, *Nucl. Instr. Meth.* **A 374** (1996), 27.

[17] A. Sharma, Ph. D. Thesis University of Geneva, Study and Optimization of the tracking Device for the FINUDA Experiment, 1996.

[18] Rob Veenhof *GARFIELD, a drift-chamber simulation program*, CERN Program Library entry W5050.

[19] E. Botta *et al.*, "A Twin Amplifier for Drift Chambers Readout" accepted for publication by *Nucl. Instr. Meth.*.

[20] 'PAW: Physics Analysis Workstation' CERN Program Library Long Write–Up Q121

[21] E. Botta "Il Sistema di Tracciamento dell'Esperimento FINUDA", Ph. D. Thesis, Università degli Studi di Torino, 1995 (unpublished).

[22] G. Charpak and F. Sauli, *Nucl. Instr. Meth.* **108** (1973), 413- -426.

[23] V. Palladino *et al.*,*Nucl. Instr. Meth.* **128** (1975), 323.
F. Sauli, *Nucl. Instr. Meth.* **156** (1978), 147–157.

[24] F. Sauli *Principles of Operation of Multi–Wire Proportional and Drift Chambers*, CERN 77–09, 3 May 1977.

[25] G. Dellacasa *et al. Nucl. Instr. Meth.* **176** (1980), 363.

[26] A. Breskin *et al.*, *Nucl. Instr. Meth.* **124** (1975), 189–214.

List of Figures

mixture components	mixture percentages	electric field (V/cm)	drift velocity (cm/μs)	σ_L (μm)
He–CH_4	90–10	1000	1.86	193.7
		1400	1.98	208.9
		2000	2.18	234.8
	80–20	1000	2.56	174.7
		1400	2.66	171.0
		2000	2.73	178.9
	70–30	1000	3.17	163.2
		1400	3.30	153.7
		2000	3.31	152.1
He–C_2H_6	90–10	1000	2.00	183.5
		1400	2.12	189.4
		2000	2.27	208.0
	80–20	1000	2.56	155.4
		1400	2.73	150.2
		2000	2.84	154.6
	70–30	1000	2.96	142.4
		1400	3.19	135.0
		2000	3.32	132.0
He–iC_4H_{10}	90–10	1000	2.32	159.3
		1400	2.50	154.9
		2000	2.62	161.8
	80–20	1000	2.78	137.5
		1400	3.09	129.4
		2000	3.30	124.1
	70–30	1000	3.03	127.3
		1400	3.43	117.6
		2000	3.73	110.4
He–CO_2	90–10	1000	2.68	141.1
		1400	3.00	139.9
		2000	3.16	167.0
	80–20	1000	2.46	126.8
		1400	3.26	125.3
		2000	3.95	124.9
	70–30	1000	2.00	113.4
		1400	2.85	119.8
		2000	3.97	143.4
He–DME	90–10	1000	2.10	159.3
		1400	2.52	154.9
		2000	2.79	161.8
	80–20	1000	1.57	141.2
		1400	2.25	138.8
		2000	3.00	132.2
	70–30	1000	1.10	125.1
		1400	1.69	126.8
		2000	2.57	125.8

Table 1: Calculated values of drift velocity and of single electron longitudinal diffusion for 1 cm drift length for some He–based mixtures as a function of the drift electric field (from [14]). Typical value of the FINUDA electric field in operating conditions is ~1400 V/cm.

	B=1.5 T	ψ (deg) for E=800 V/cm	ψ (deg) for E=1000 V/cm	ψ (deg) for E=2000 V/cm
Ar–CH_4				
	90–10	79.63	72.26	34.26
	80–20	82.43	79.33	49.70
He–DME				
	90–10	18.85	18.14	13.37
	80–20	13.16	13.6	13.21
	70–30	9.30	9.85	11.23
He–iC_4H_{10}				
	90–10	26.06	23.13	13.86
	80–20	29.02	26.64	17.68
	70–30	30.08	28.16	19.97
	B = 1.1 T			
He–iC_4H_{10}				
	70–30	22.78	21.19	14.71

Table 2: Comparison of Lorentz angles ψ for some He–based mixtures at B=1.5 T for three values of the electric field (from [14]). Values at B=1.1 T for the He–iC_4H_{10} (70%–30%) mixture are also reported. For electric and magnetic field values typical of our operating conditions (E$\sim$1400 V/cm and B=1.1 T) the calculated Lorentz angle is 18.27°.

	$\bar{z}$ (cm)	$\bar{z}$ (cm)
no corr.	–2.68±0.51	–32.45±0.96
k_{mean}	–3.25±0.62 (0.5%)	–42.56±1.25 (1.09%)
k(t)	–3.75±0.68 (0.6%)	–45.22±1.24 (1.08%)
k2(t)		–43.44±1.11 (0.91%)
hw. corr.	–3.96±0.32 (0.28%)	–39.78±0.39 (0.34%)

Table 3: Summary of measured and corrected $z-$coordinate values: no correction (no corr.) refers to the measured values without any correction, k_{mean} to the values obtained applying the correction of (7), k(t) and k2 (t) to the values obtained with two different software corrections taking into account the drift time and, finally, hardware correction (hw. corr.) to the values measured with an integration gate of 200 ns. The measurements were performed at 4 cm and 44 cm from the center of the wire respectively (columns 2 and 3).

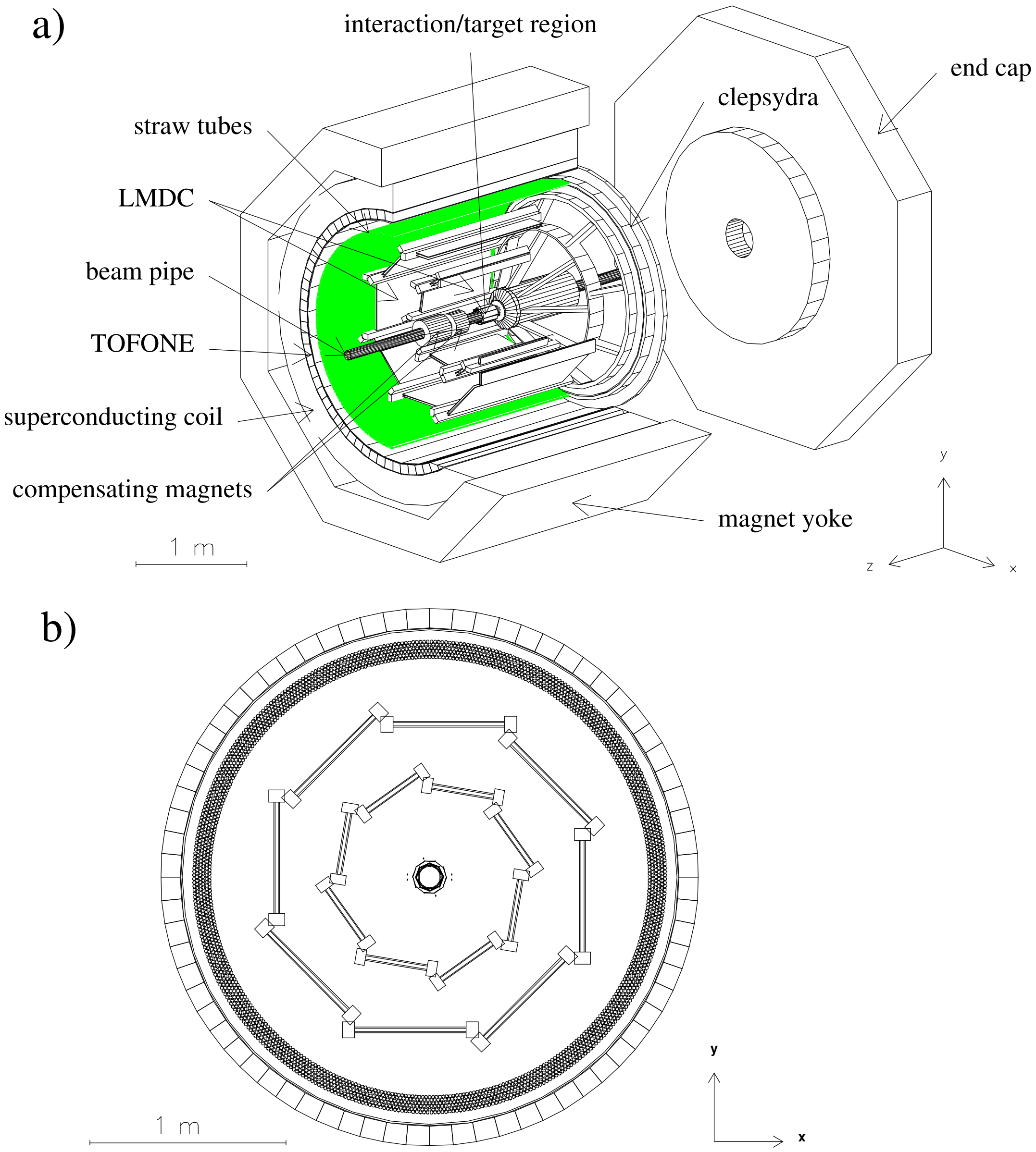
a)
interaction/target region
end cap
clepsydra
straw tubes
LMDC
beam pipe
TOFONE
superconducting coil
compensating magnets
magnet yoke
1 m
y
z
x
b)
1 m
y
x

Figure 1:

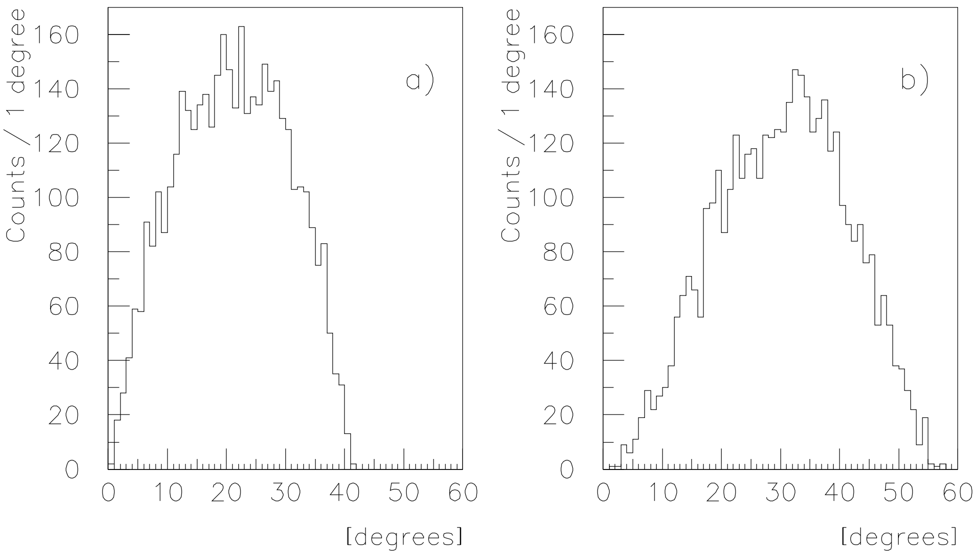
Counts / 1 degree
160
140
120
100
80
60
40
20
0
0 10 20 30 40 50 60
[degrees]
a)
Counts / 1 degree
160
140
120
100
80
60
40
20
0
0 10 20 30 40 50 60
[degrees]
b)

Figure 2:

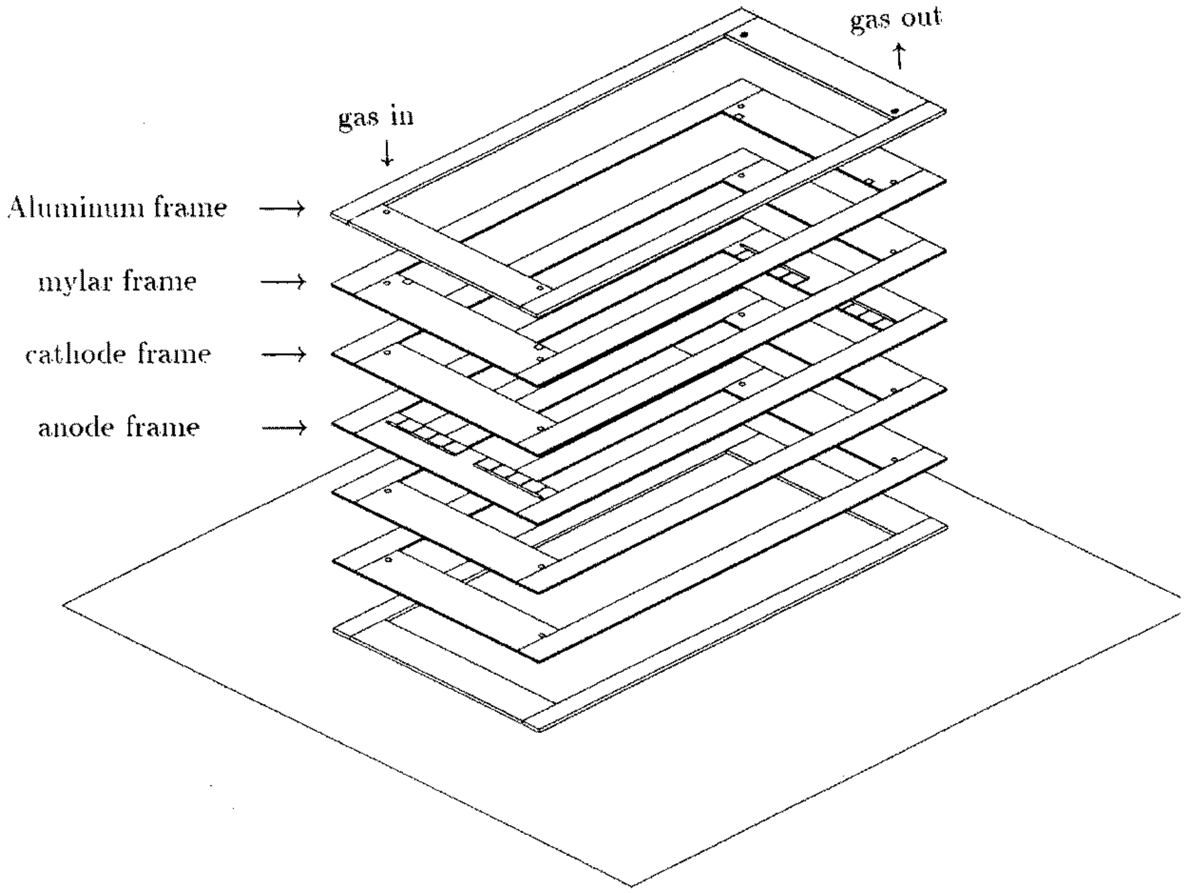
gas out
gas in
Aluminum frame
mylar frame
cathode frame
anode frame

Figure 3:

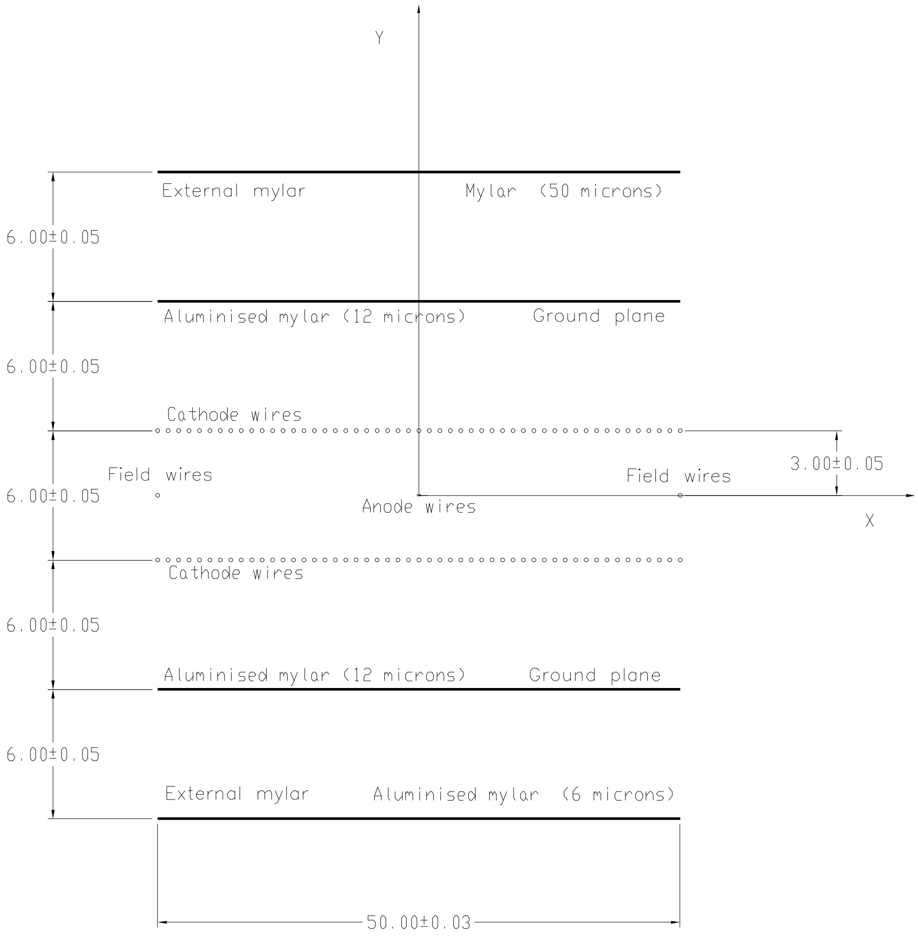

Y
External mylar
Mylar (50 microns)
6.00±0.05
Aluminised mylar (12 microns)
Ground plane
6.00±0.05
Cathode wires
3.00±0.05
Field wires
Field wires
6.00±0.05
Anode wires
X
Cathode wires
6.00±0.05
Aluminised mylar (12 microns)
Ground plane
6.00±0.05
External mylar
Aluminised mylar (6 microns)
50.00±0.03

Figure 4:

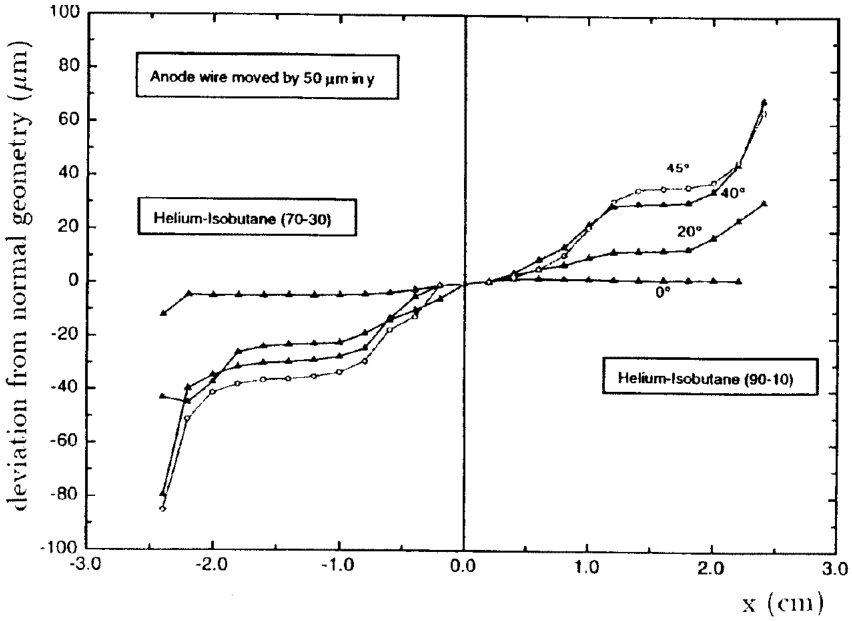

Anode wire moved by 50 μm in y
Helium-Isobutane (70-30)
Helium-Isobutane (90-10)
45°
40°
20°
0°
deviation from normal geometry (μm)
x (cm)
100
80
60
40
20
0
-20
-40
-60
-80
-100
-3.0
-2.0
-1.0
0.0
1.0
2.0
3.0

Figure 5:

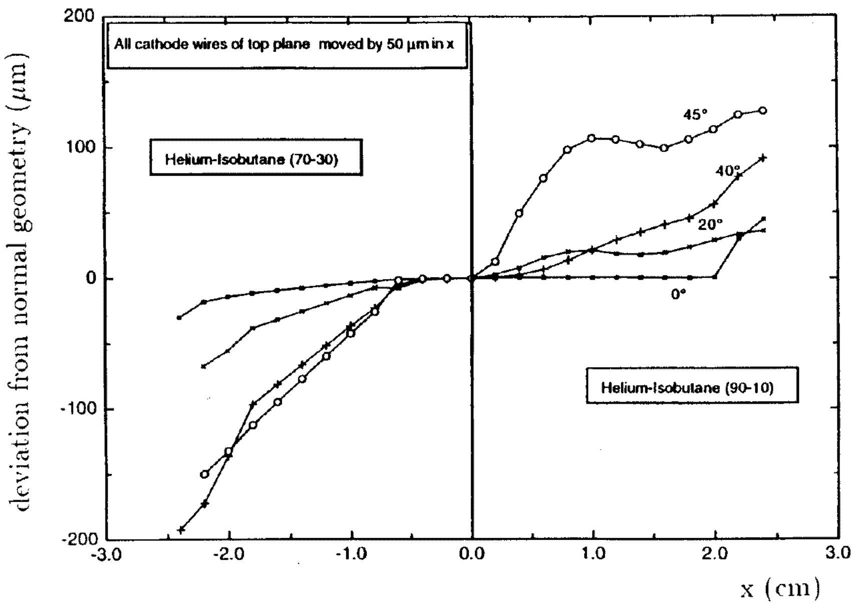
All cathode wires of top plane moved by 50 μm in x
Helium-Isobutane (70-30)
Helium-Isobutane (90-10)
45°
40°
20°
0°
200
100
0
-100
-200
-3.0
-2.0
-1.0
0.0
1.0
2.0
3.0
deviation from normal geometry (μm)
x (cm)

Figure 6:

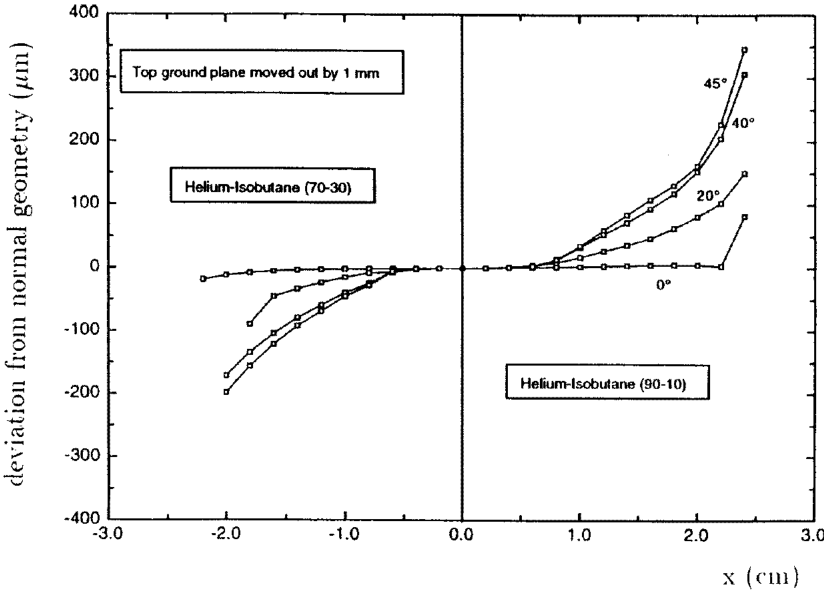

Top ground plane moved out by 1 mm
Helium-Isobutane (70-30)
Helium-Isobutane (90-10)
45°
40°
20°
0°
deviation from normal geometry (μm)
x (cm)

Figure 7:

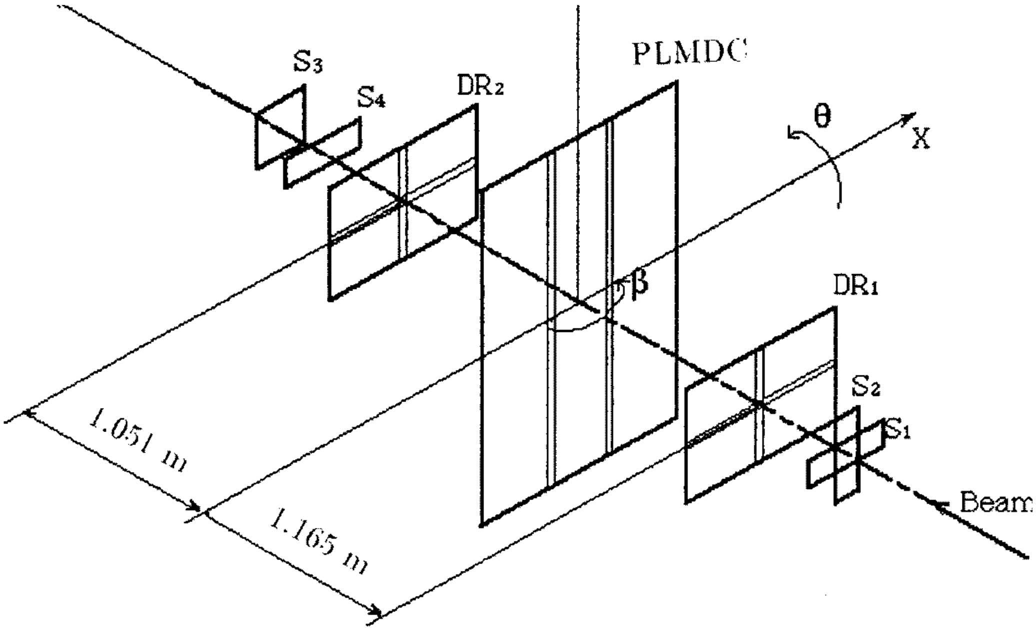

Figure 8:

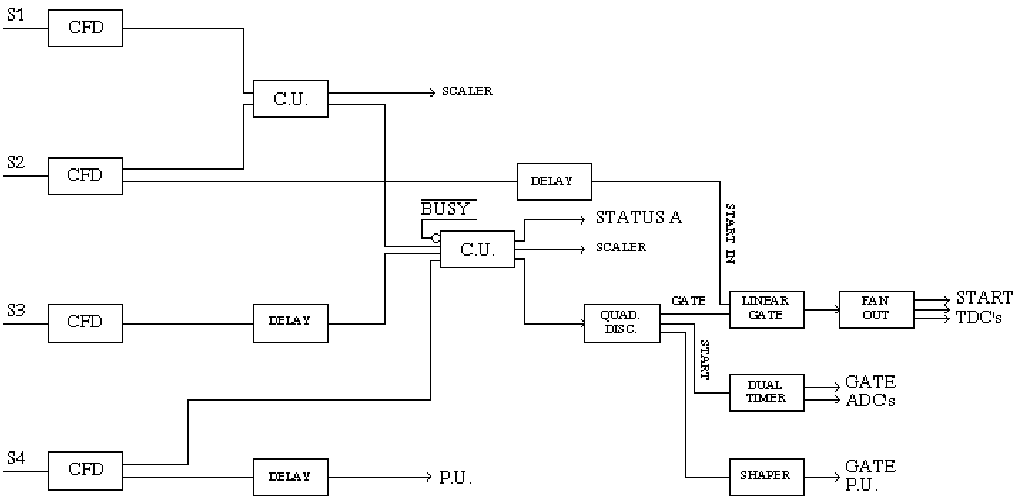
S1
CFD
C.U.
SCALER
S2
CFD
DELAY
BUSY
STATUS A
START IN
C.U.
SCALER
S3
CFD
DELAY
QUAD. DISC.
GATE
LINEAR GATE
FAN OUT
START TDC's
START
DUAL TIMER
GATE ADC's
S4
CFD
DELAY
P.U.
SHAPER
GATE P.U.

Figure 9:

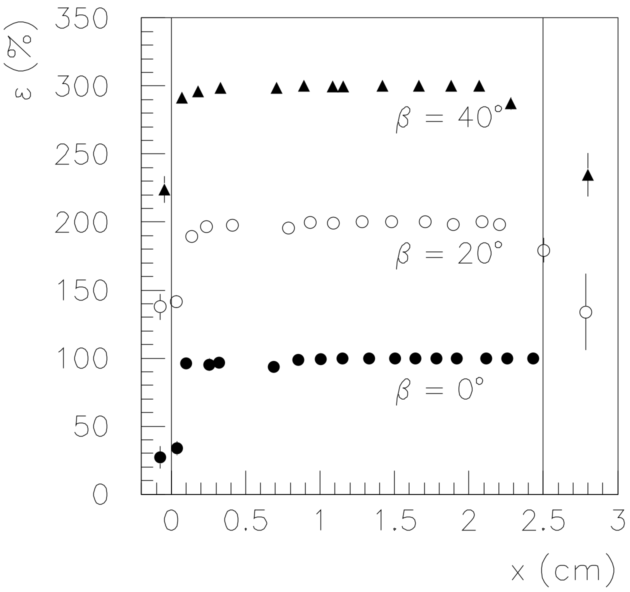

Figure 10:

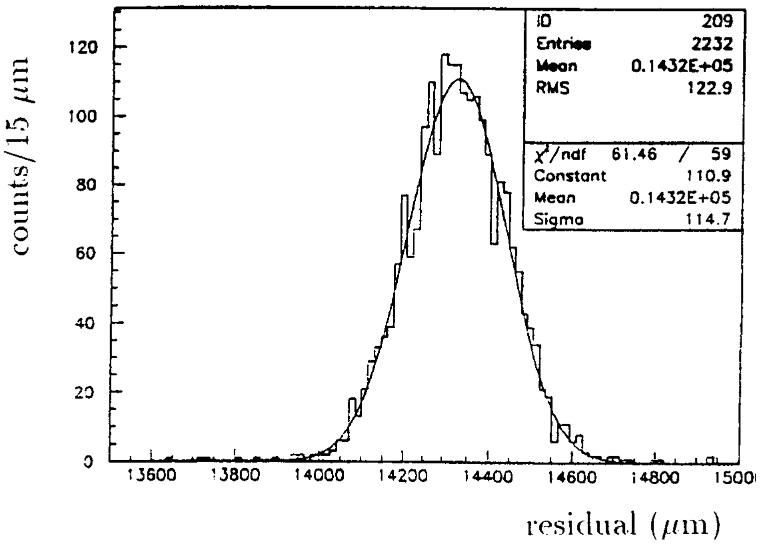

counts/15 μm
ID 209
Entries 2232
Mean 0.1432E+05
RMS 122.9
χ²/ndf 61.46 / 59
Constant 110.9
Mean 0.1432E+05
Sigma 114.7
0
20
40
60
80
100
120
13600
13800
14000
14200
14400
14600
14800
15000
residual (μm)

Figure 11:

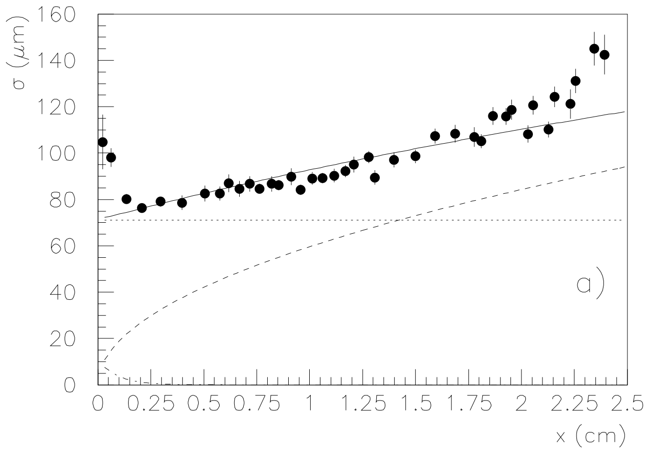

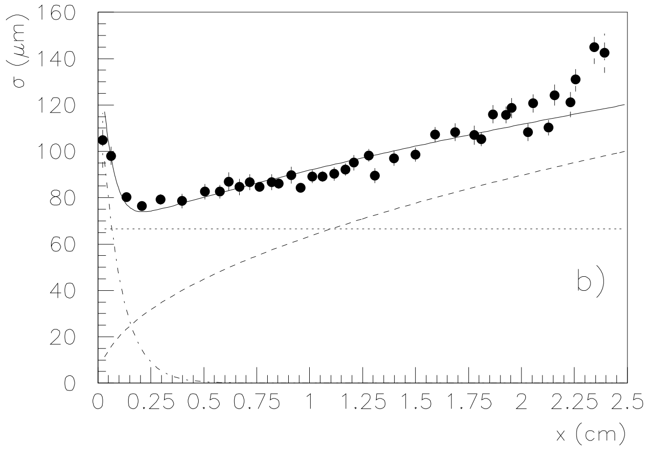

Figure 12:

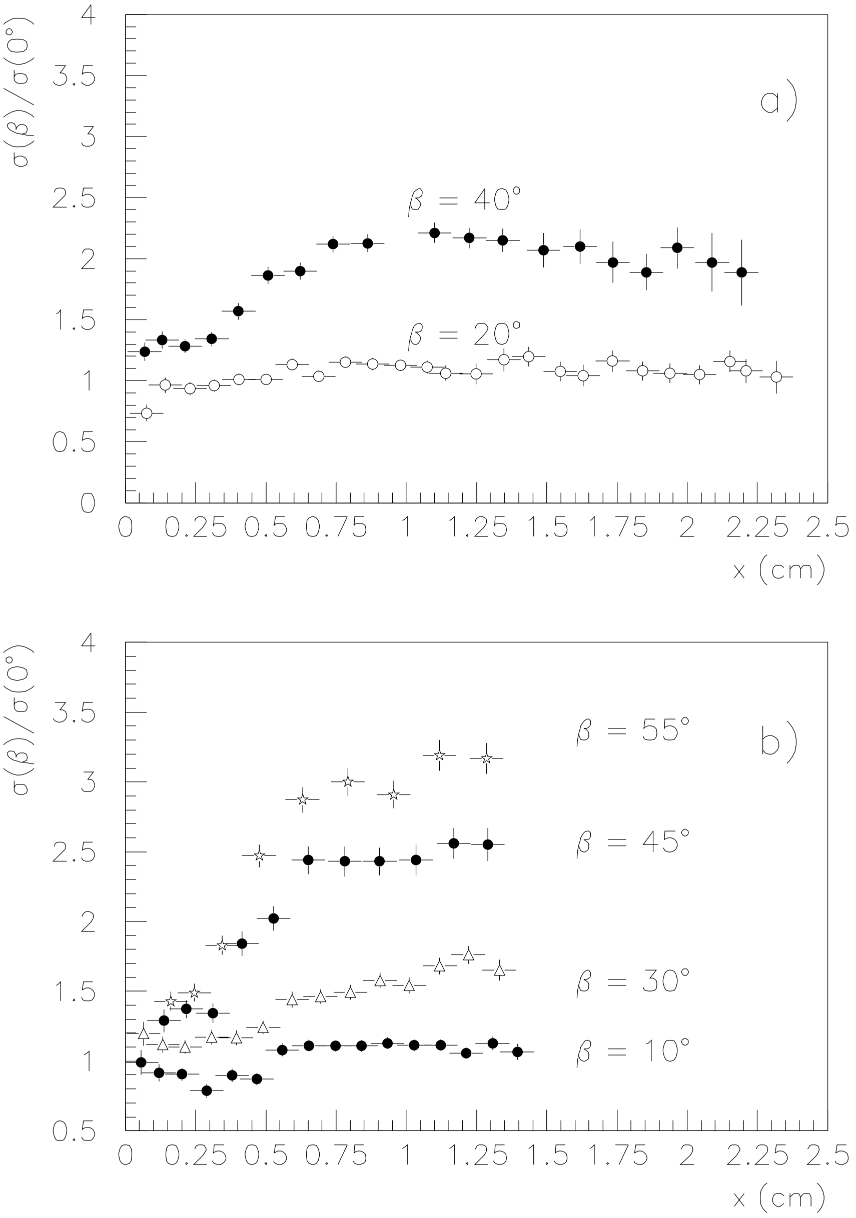

Figure 13:

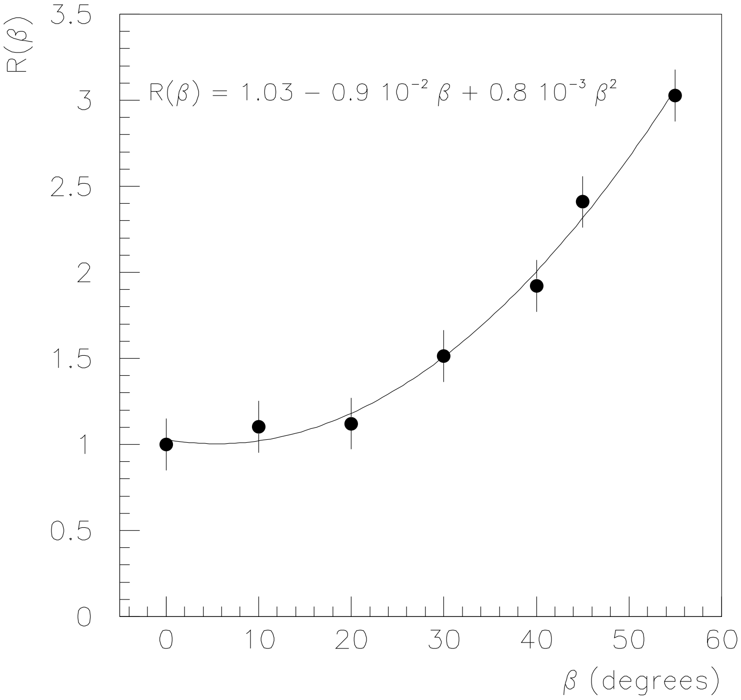

R(β)
R(β) = 1.03 − 0.9 10⁻² β + 0.8 10⁻³ β²
3.5
3
2.5
2
1.5
1
0.5
0
0
10
20
30
40
50
60
β (degrees)

Figure 14:

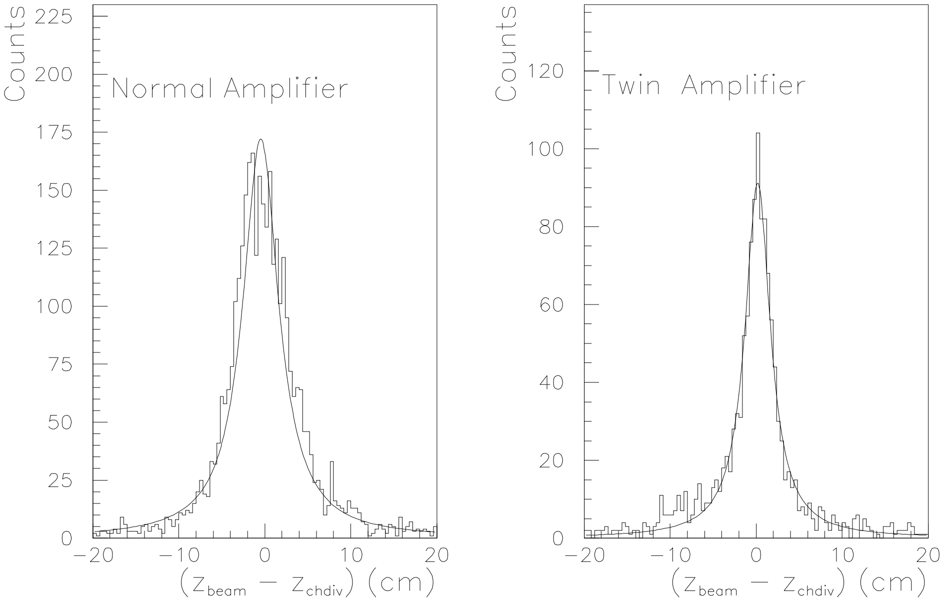
Normal Amplifier
Counts
225
200
175
150
125
100
75
50
25
0
−20
−10
0
10
20
(Z_beam − Z_chdiv) (cm)
Twin Amplifier
Counts
120
100
80
60
40
20
0
−20
−10
0
10
20
(Z_beam − Z_chdiv) (cm)

Figure 15:

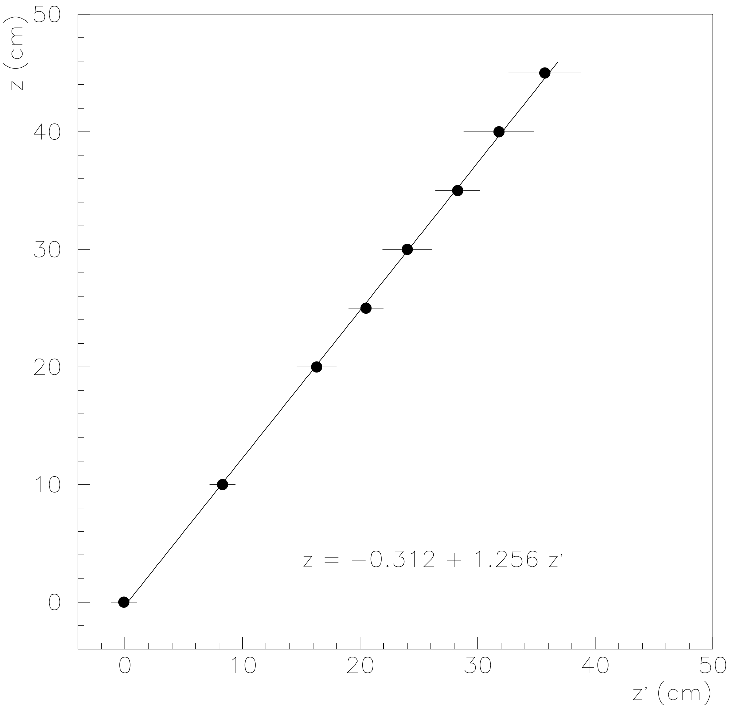

Figure 16:

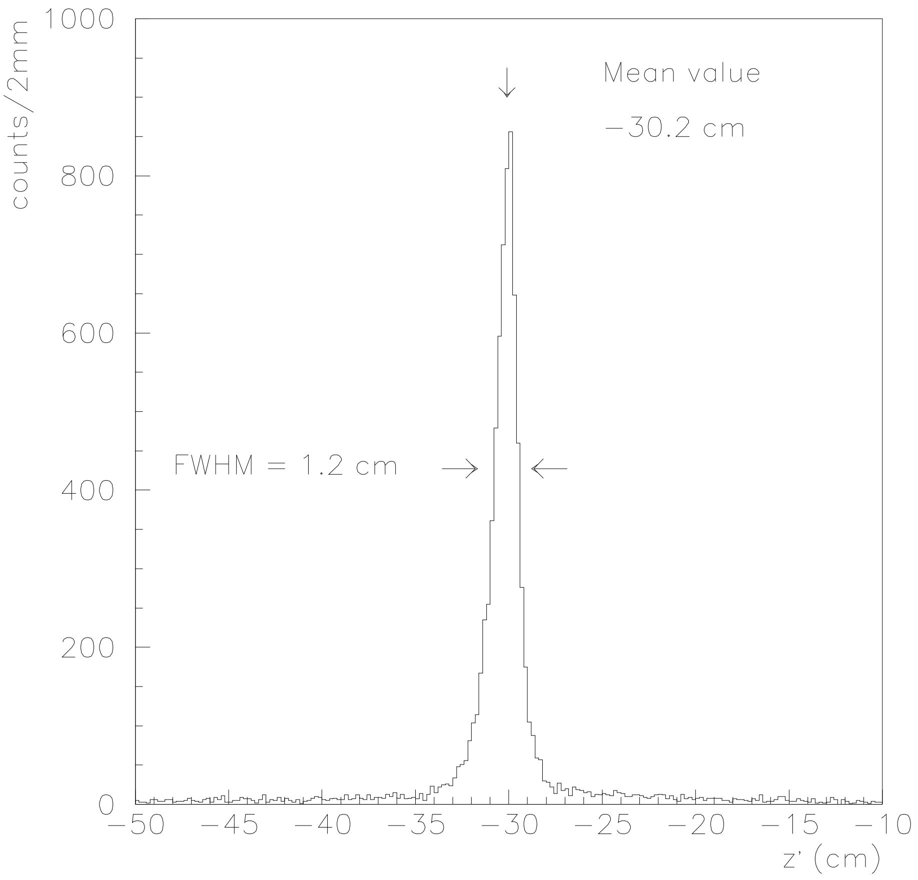

counts/2mm
1000
800
600
400
200
0
Mean value
−30.2 cm
FWHM = 1.2 cm
−50 −45 −40 −35 −30 −25 −20 −15 −10
z' (cm)

Figure 17:

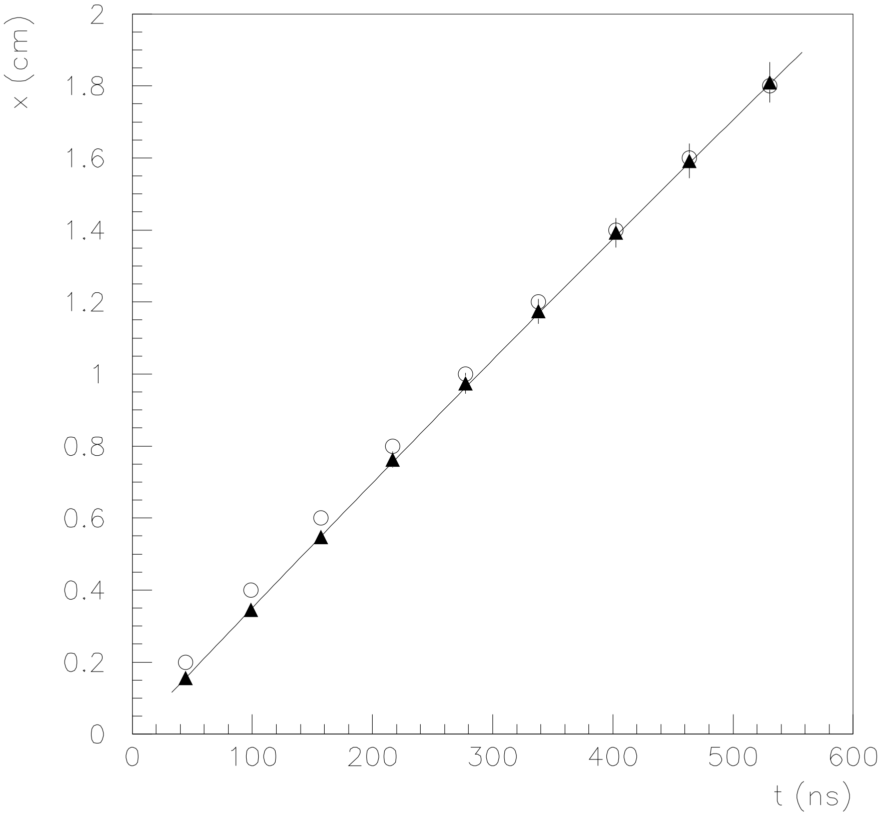

Figure 18: